ACS Catalysis

Open Access

pubs.acs.org/acscatalysis

Research Article

Bimetallic Mn_xRu_{100-x} Nanoparticles on Supported Ionic Liquid Phases (Mn_xRu_{100-x}@SILP) as Tunable Hydrogenation Catalysts

Johannes Zenner, Liqun Kang, Neha Antil, Jacob Johny, Serena DeBeer, Walter Leitner,* and Alexis Bordet*

Cite This: *ACS Catal.* 2025, 15, 3227−3235

Read Online

ACCESS | Metrics & More | Article Recommendations | Supporting Information

ABSTRACT: Bimetallic manganese−ruthenium nanoparticles of defined Mn:Ru ratios were prepared on an imidazolium-based supported ionic liquid phase. Characterization of the resulting Mn_xRu_{100-x}@SILP materials by electron microscopy evidenced the formation of small (1.3−3.6 nm) and well-dispersed nanoparticles (NPs) containing Mn and Ru in the expected ratios. X-ray absorption spectroscopy (XAS) studies revealed that no significant levels of alloying occurred in these NPs that contain mainly oxidized Mn species and metallic Ru, consistent with the immiscibility of the two metals and the high oxophilicity of Mn. The hydrogenation performance of Mn_xRu_{100-x}@SILP materials was probed using benzylideneacetone as model substrate containing three distinct reducible moieties. Albeit the two metals are present in distinct phases, the Mn:Ru ratio was found to have a strong impact on activity and selectivity with trends similar to what was previously reported for alloyed Fe_xRu_{100-x}@SILP and Co_xRu_{100-x}@SILP catalysts. In particular, a sharp switch of 6-membered aromatic ring hydrogenation between $Mn_{15}Ru_{85}$ (full ring hydrogenation) and $Mn_{25}Ru_{75}$ (no ring hydrogenation) was observed. These results demonstrate that alloying is not a requirement to observe synergistic effects from the combination of 3d metals and noble metals in NPs, opening new opportunities for the development of bimetallic catalysts for selective hydrogenation.

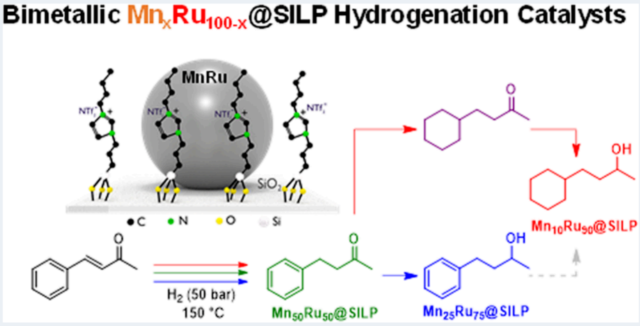

KEYWORDS: *manganese, ruthenium, bimetallic nanoparticles, supported ionic liquid phase, hydrogenation*

1. INTRODUCTION

Controlling selectivity in hydrogenation is an important design challenge for catalysis as it improves reaction efficiency, simplifies product separation, and reduces waste generation in many chemical processes.[1−6] In heterogeneous catalysis, typical strategies to tune the reactivity of surface active sites rely for example on selective poisoning (e.g., Lindlar catalyst for alkyne to alkene hydrogenation),[1,7−9] on metal−support interactions (e.g., $Cu/ZnO/Al_2O_3$ for CO_2 hydrogenation to methanol),[10−13] and on alloying (e.g., Raney nickel, a Ni−Al alloy).[14−16] These strategies aim in particular at tuning the activation mode of H_2 (homolytic versus heterolytic), as well as the interactions between reducible moieties and catalytically active sites. For example, the hydrogenation of polarized functional groups such as carbonyls is favored by polarized H_2 activation, and such functionalities are better adsorbed on and activated by oxophilic sites.[4,17] In contrast, the hydrogenation of aromatic rings typically requires planar adsorption on a surface arrangement of 3−4 noble metal atoms (i.e., Ru, Rh) that provides homolytic H_2 cleavage.[18,19]

In this context, the combination of noble metals with their base metal 3d congeners in bimetallic NPs has proven to be an effective strategy to prepare hydrogenation catalysts with tunable activity and selectivity.[4,20−27] Focusing on examples where Ru is the noble metal, changing the Fe:Ru ratio in bimetallic FeRu NPs was shown to impact activity and selectivity in Fischer−Tropsch synthesis (e.g., 40% C_{5+} products with $Fe_{25}Ru_{75}$ NPs),[23] and CO_2 hydrogenation to formic acid.[24] Tang et al. found that $Co_{12}Ru_{88}$ NPs supported on TiO_2 were 2.1 times more active than monometallic Ru NPs of similar size for the hydrogenation of CO_2 to methanol.[27] Our group has shown that imidazolium-based supported ionic liquid phases (SILPs) are particularly suitable for the immobilization and stabilization of bimetallic 3d metal-noble metal NPs.[28−35] Such SILPs have been shown to provide various benefits in catalysis, such as controlled NPs growth, improved NPs stability, tunable wettability, and the possibility to introduce additional functionalities.[28,36−38] For example, Co_xRh_{100-x}@SILP[32] and M_xRu_{100-x}@SILP (M = Fe, Co)[29,34]

Received: September 9, 2024
Revised: January 8, 2025
Accepted: January 13, 2025
Published: February 7, 2025

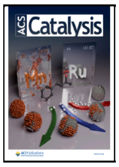

https://doi.org/10.1021/acscatal.4c05494

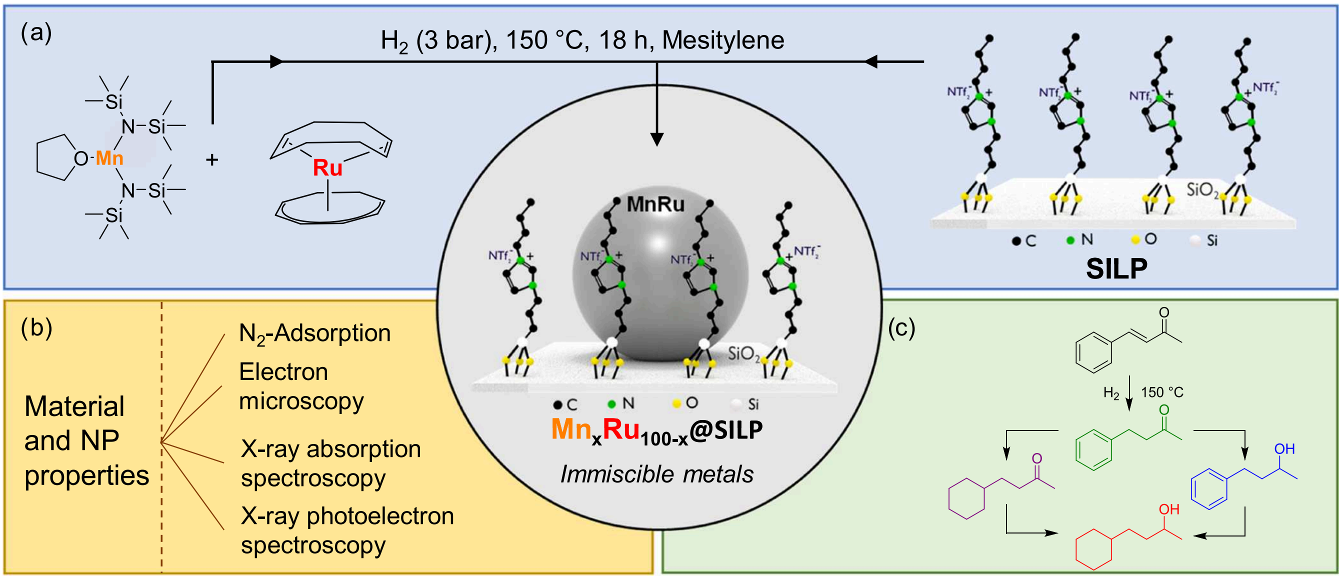

Figure 1. Methodology followed in this study. (a) Synthesis of bimetallic MnRu nanoparticles (NPs) on supported ionic liquid phases; (b) characterization of the resulting Mn_xRu_{100-x}@SILP materials; (c) model reaction and reaction network used to evaluate hydrogenation performance of Mn_xRu_{100-x}@SILP.

catalysts, in which the two metals form alloy-type NPs, were applied to the hydrogenation of multifunctional aromatic substrates (e.g., benzylideneacetone, bicyclic heteroaromatics, etc.), evidencing strong synergistic effects with activities and selectivities inaccessible to the individual metals. Interestingly, the nature of the "diluting" 3d metal was found to finetune the catalytic properties, but the same general trends were observed for suppression of aromatic ring hydrogenation and enhancement of C═O hydrogenation.[29,34]

These tunable effects are still poorly understood at the fundamental level. While previous reports focused on combinations of metals that produced alloyed NPs, we selected for the present study manganese (Mn) and ruthenium (Ru), two immiscible metals.[39,40] The immobilization of noble metal NPs on manganese oxide has been previously explored by Manyar et al. and McManus et al., using Pt NPs on a porous manganese oxide (OMS-2) for the hydrogenation of C═C and nitro groups.[41,42] However, reports on the preparation of bimetallic NPs of Mn and a noble metal such as Ru are extremely scarce,[43−45] and such NPs have so far not been applied as hydrogenation catalysts. The abundance and low environmental impact of Mn,[46,47] and the excellent hydrogenation performance of some Mn-based organometallic catalysts[48−51] make this apparent lack of knowledge on combining Mn and Ru for catalytic applications particularly intriguing.

Thus, we present herein the preparation of a series of Mn_xRu_{100-x}@SILP catalysts, their characterization, and application for a model hydrogenation reaction. Mn_xRu_{100-x} NPs with a wide range of tunable compositions were synthesized following an organometallic approach involving the coreduction of a Mn and Ru complex under mild conditions in the presence of the SILP (Figure 1a). The resulting materials were characterized by a variety of methods, including electron microscopy and X-ray absorption spectroscopy (XAS) techniques to determine NP size, elemental composition and oxidation states, with a specific focus on the interaction between Mn and Ru in the NPs (Figure 1b). The influence of the Mn:Ru ratio on the catalytic performances was evaluated in the hydrogenation of benzylideneacetone, a prototypical example for substrates with several potentially reducible moieties (Figure 1c). Comparison with previously reported FeRu and CoRu alloys provided additional insight into the influence of the composition and structure of bimetallic NPs on their catalytic properties.

2. MATERIALS AND METHODS

2.1. Synthesis. The imidazolium-based SILP was prepared according to a previously published procedure.[29] In brief, the ionic liquid [1-butyl-3-(3-triethoxysilylpropyl)-imidazolium]-NTf_2 (NTf_2 = bis(trifluoromethanesulfonyl)imide) was chemisorbed onto dehydroxylated SiO_2 (500 °C for 16 h in vacuo) via a silanization reaction. This SILP was demonstrated to be suitable for the synthesis and stabilization of various mono- and bimetallic NPs used for hydrogenation[19,29,32,34] and hydrodeoxygenation reactions,[31,33] and is thermally stable up to 350 °C.[19] Notably, our group recently employed this SILP for the stabilization of monometallic Mn NPs applied to catalytic transfer hydrogenation reactions.[52] Mn_xRu_{100-x} NPs were immobilized on the SILP following an organometallic approach involving the in situ reduction of $[Mn[N(SiMe_3)_2]_2(THF)]$ (THF = tetrahydrofuran) and [Ru(cod)(cot)] (cod = 1,5-cyclooctadiene; cot = 1,3,5-cyclooctatriene) in the presence of the SILP in mesitylene under an atmosphere of H_2 (3 bar) at 150 °C over 18 h, giving Mn_xRu_{100-x}@SILP materials with a theoretical total metal loading of 1 mol %. The selected organometallic metal complexes were chosen based on a combination of stability during handling and ligand lability upon hydrogenation, allowing the formation of well-defined NPs with a clean surface and tunable composition (x = 0, 10, 15, 25, 33, 50, 75, 100).

2.2. Characterization. N_2-adsorption studies of Mn_xRu_{100-x}@SILP materials showed Brunauer−Emmett−Teller (BET) surface areas in the 200−265 $m^2\ g^{-1}$ range (Table S1). The observed decrease in surface area as compared to the starting dehydroxylated silica support material (342 $m^2\ g^{-1}$) is expected due to the surface coverage by the chemisorbed ionic

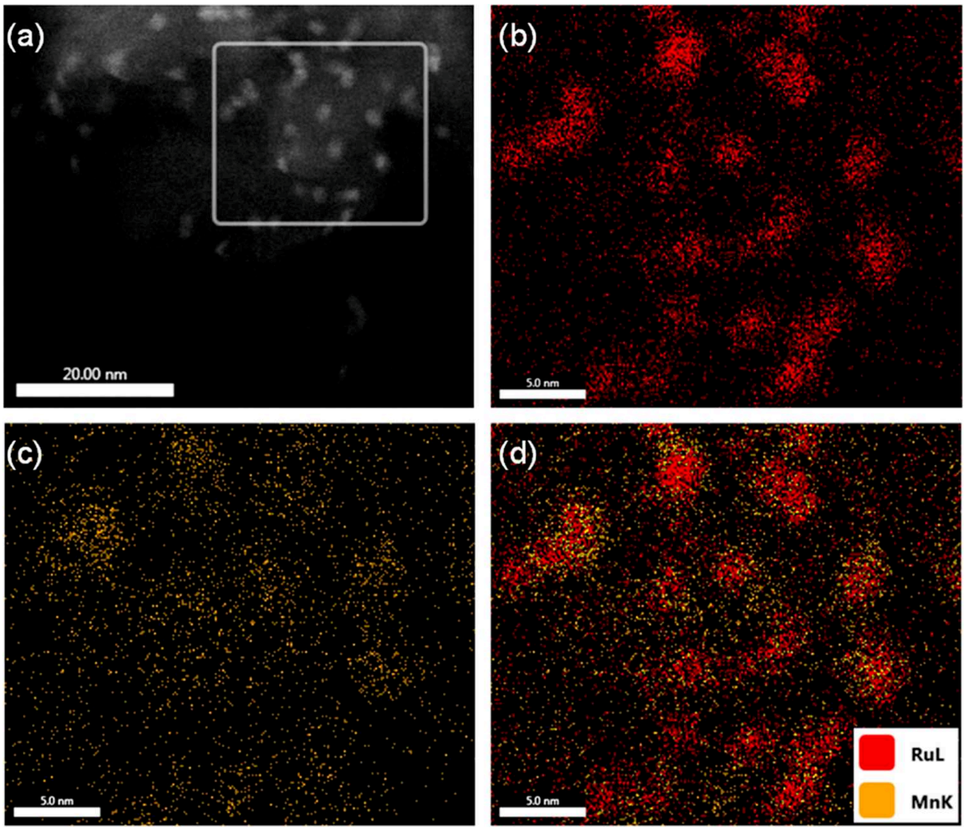

Figure 2. (a) STEM-HAADF image of $Mn_{25}Ru_{75}$@SILP with EDX elemental mappings of (b) Ru Lα and (c) Mn Kα; (d) overlay of Ru and Mn. For EDX spectrum see Figure S9.

liquid-like layer. Metal loadings and Mn:Ru ratios were determined by scanning electron microscopy with energy dispersive X-ray spectroscopy (SEM-EDX) and are in excellent agreement with theoretical values (Table S2). Mn_xRu_{100-x}@SILP materials were further characterized by transmission and scanning transmission electron microscopy (TEM and STEM, respectively), showing the presence of small (1−4 nm) and well-dispersed NPs (examples in Figures 2 and S1−S6, summary provided in Table S2) in all cases irrespective of the Mn:Ru ratio, with a few aggregates visible in some materials. Interestingly, the smallest NPs were observed on $Mn_{50}Ru_{50}$@SILP (1.3 ± 0.4 nm, Figure S5). NPs size progressively increased with the increase in Mn content (up to 2.0 nm for Mn_{100}@SILP) or Ru content (up to 3.6 nm for Ru_{100}@SILP). Such trend was not observed for Fe_xRu_{100-x}@SILP, Co_xRu_{100-x}@SILP and Co_xRh_{100-x}@SILP materials prepared by a similar approach.[29,32,34]

Elemental mappings of Mn and Ru using STEM-HAADF-EDX (HAADF = high-angle annular dark-field) showed the presence of NPs containing both Mn and Ru (Figures 2 and S7−S9), indicating the successful preparation of bimetallic Mn_xRu_{100-x} NPs on the SILP support. Interestingly, NPs were more agglomerated and not bimetallic when using unmodified SiO_2 instead of the SILP as a support (Figures S10−S11), presumably due to the sensitivity of the $[Mn[N(SiMe_3)_2]_2(THF)]$ precursor toward the SiO_2 surface.

$Mn_{25}Ru_{75}$@SILP was further investigated using aberration-corrected STEM with atomic resolution (Figure S12) and lattice parameters of the NPs were determined by fast-Fourier-transform. The found lattice parameters (mainly 2.07 Å, less often 1.36, 2.36, and 1.59 Å) are all in accordance with hexagonal Ru ($P6_3/mmc$).[53] No lattice structure belonging to crystalline Mn species could be observed through this local analysis, meaning that Mn atoms may be integrated in the Ru lattice, and/or present in amorphous structures in the NPs. However, beam damage during measurement cannot be excluded.

The oxidation states and alloying properties of Mn and Ru species in Mn_xRu_{100-x}@SILP materials (x = 10, 15, 25, 50) were investigated by XAS (Figure 3). Detailed information on data collection, processing and analysis is detailed in the SI (Including Figure S13−S20 and Tables S3−S4). In brief, Mn K-edge X-ray absorption near edge structure (XANES) spectra of Mn_xRu_{100-x}@SILP materials (Figure 3a) are shifted to higher energies as compared to metallic Mn, and point toward an oxidation state similar to Mn^{2+} in MnO. Ru K-edge XANES are similar for all Mn_xRu_{100-x}@SILP materials (Figure 3b), indicating zerovalent Ru NPs with only trace amount of oxidation, and suggesting that the average oxidation states of Mn species are largely consistent regardless of the Mn−Ru ratio. Mn K-edge extended X-ray absorption fine structure (EXAFS) analysis (Figure 3c and Table S3) evidenced highly disordered Mn-species, with coordination numbers (C.N.) dominated by Mn−O interactions (C.N. = 5.5−6), followed by Mn−Mn (C.N. = 1−2) and Mn−Ru (C.N. = 0.2−1.4). Ru K-edge EXAFS (Figure 3d and Table S4) revealed large Ru−Ru C.N. (8−9) and low Ru−Mn C.N. (0.1−2.2).

These results indicate that only small portions of Mn and Ru species are present as a MnRu alloy in Mn_xRu_{100-x}@SILP materials, as was expected due to the known mismatch between the crystal structures of metallic Mn ($I\bar{4}3m$) and Ru ($P6_3/mmc$).[39,40] While remaining Mn and Ru species are in

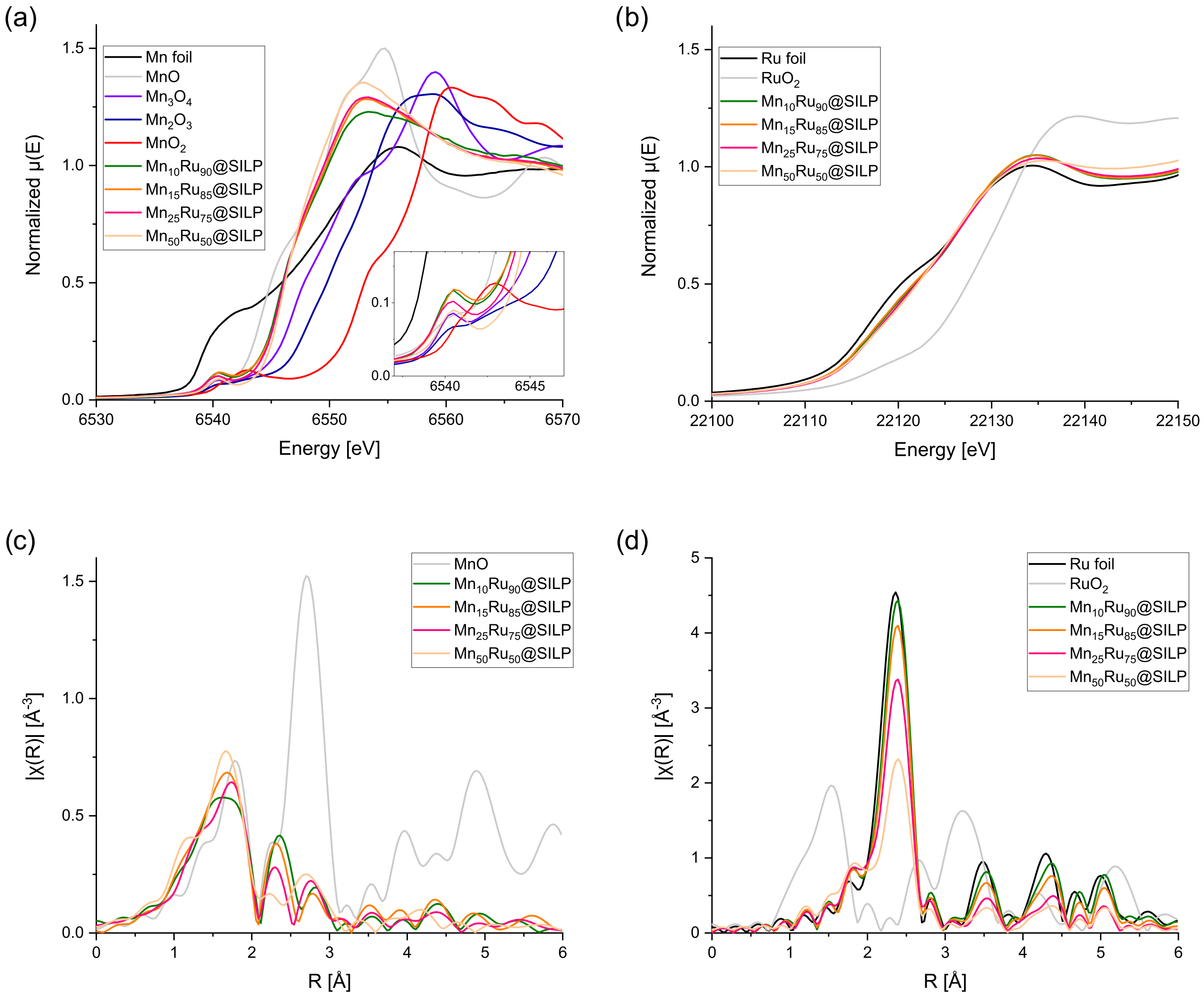

Figure 3. XAS analysis of Mn_xRu_{100-x}@SILP. Comparison of normalized (a) Mn K-edge and (b) Ru K-edge XAS for x = 10, 15, 25, 50 with Mn- and Ru-based reference materials and comparison of normalized (c) Mn K-edge and (d) Ru K-edge EXAFS in R-space for x = 10, 15, 25, 50 with Mn- and Ru-based reference materials. EXAFS spectra were generated by Fourier transform of the k-space from k = 0−6 Å^{-1}. EXAFS data were k^2-weighted.

separate phases, they are still present together in bimetallic NPs, as shown by STEM-HAADF-EDX analysis. Based on these characterization data, the notation "Mn_xRu_{100-x}@SILP" will from now on refer to nonalloyed bimetallic NPs containing metallic Ru and oxidized Mn species. The elemental and chemical states of $Mn_{25}Ru_{75}$@SILP were further examined using X-ray photoelectron spectroscopy (XPS). Figure S21a presents the high-resolution XPS spectrum for Ru 3p, where the Ru $3p_{3/2}$ and Ru $3p_{1/2}$ peaks appear at binding energies of 461.9 and 483.8 eV, respectively. These values align well with literature values for metallic Ru,[54] supporting XANES findings. The Mn 2p spectrum (Figure S21b) reveals the characteristic Mn $2p_{3/2}$ and Mn $2p_{1/2}$ peaks at 642.3 and 654.1 eV, indicative of oxidized Mn.[54] These observations confirm the presence of metallic Ru alongside oxidized Mn in the $Mn_{25}Ru_{75}$@SILP material. Additionally, F 1s and N 1s XPS spectra were investigated to gather information on the ionic liquid. The F 1s peak at 689.0 eV (Figure S21c) is characteristic of the NTf_2 anion, and the two N 1s components at 400.0 and 402.1 eV (Figure S21d) are assigned to the anion and cation parts of the ionic liquid.[55]

2.3. Catalysis. Benzylideneacetone (**1**) was selected as a model substrate to test the hydrogenation performance (activity and selectivity) of Mn_xRu_{100-x}@SILP materials. **1** possesses an aromatic ring, a conjugated double bond, and a nonbenzylic ketone, giving the opportunity to probe the reactivity of Mn_xRu_{100-x}@SILP for a whole range of prototypical functional groups. Therefore, the hydrogenation of **1** can lead to several different products (Figure 4) through a sequence of consecutive and parallel hydrogenation reactions: 4-phenylbutan-2-one (**1a**), 4-cyclohexylbutan-2-one (**1b**), 4-phenylbutan-2-ol (**1c**) and 4-cyclohexylbutan-2-ol (**1d**). The hydrogenation of **1** was also the model reaction in previous investigations of bimetallic catalysts such as FeRu@SILP, CoRu@SILP, and CoRh@SILP. Figure 4 depicts the product distribution of the hydrogenation of **1** using Mn_xRu_{100-x}@SILP catalysts with different Mn:Ru ratios. Reactions were carried out under a set of standard reaction conditions (100 equiv of **1** respective to the total molar amount of metal in the

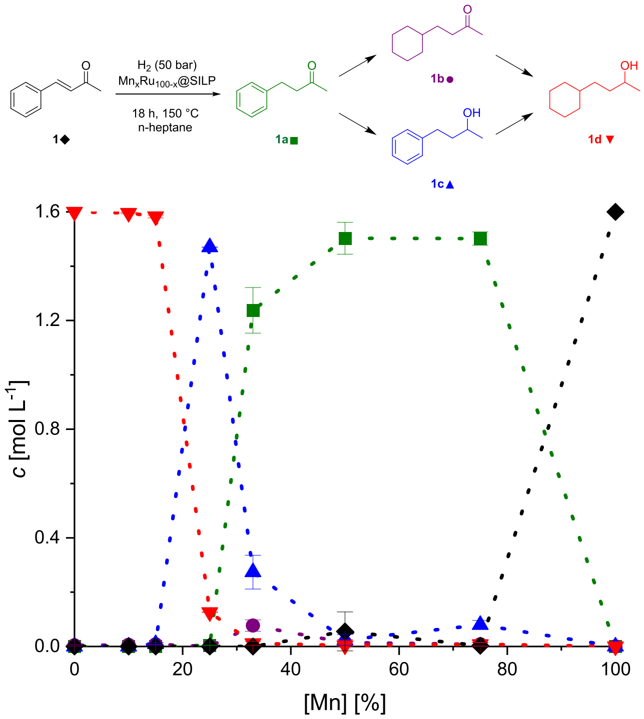

Figure 4. Hydrogenation of **1** using a series of Mn_xRu_{100-x}@SILP catalysts with different Mn:Ru metal ratios. Reaction conditions: Mn_xRu_{100-x}@SILP (20 mg, 0.008 mmol metals), benzylideneacetone (117 mg, 0.8 mmol, 100 equiv), 150 °C, 18 h, *n*-heptane (0.5 mL). Yields are determined via GC-FID using tetradecane as an internal standard. See Table S6 for the complete data set. Data points are average values of 2−4 experiments, and error bars represent standard deviations.

catalysts, in *n*-heptane at 150 °C under H_2 (50 bar)) that were selected to facilitate direct comparison with previously reported FeRu@SILP and CoRu@SILP systems (Figure S22) with fully alloyed NPs.[34]

Monometallic Ru_{100}@SILP gave quantitative yield of the fully hydrogenated product **1d**, which is consistent with the expected reactivity of Ru NPs under these conditions.[29] Incorporation of small amounts of Mn up to $Mn_{15}Ru_{85}$ did not change this selectivity significantly, and only traces of **1c** or **1b** (<1%) were detected in the product mixtures. Interestingly, increasing the Mn content to 25% in $Mn_{25}Ru_{75}$@SILP resulted in the suppression of the aromatic ring hydrogenation activity and in a sharp switch to **1c** as main product (92%). This effect can be tentatively attributed to an increase in Mn concentration at the surface of the bimetallic NPs, diluting the Ru and making the existence of ensembles of 3−4 Ru atoms required for aromatic ring adsorption unlikely.[18] This "isolation" of Ru atoms by MnO_x phases at the surface of the bimetallic NPs results in a reactivity that resembles that of homogeneous or single-site catalysts.[56] Further increasing the Mn content to 33% slowed down the ketone hydrogenation, and led to **1a** as main product (77%). For higher Mn contents ($Mn_{50}Ru_{50}$ and $Mn_{75}Ru_{25}$), the ketone hydrogenation was completely shut down, and only C═C hydrogenation to produce **1a** (94% and 95%, respectively) was observed. Monometallic Mn_{100}@SILP was inactive in the hydrogenation of **1**, presumably due to oxidation of the Mn NPs on the oxygen-rich support.[52] Using the $Mn_{25}Ru_{75}$@SiO_2 reference catalyst in the hydrogenation of **1** under standard reaction conditions gave quantitative yield of the fully saturated 4-cyclohexylbutan-2-ol (**1d**) product (Table S6), consistent with the presence of monometallic Ru and Mn NPs in the catalyst. As expected, the SILP alone possesses negligible activity (Table S6).

Intriguingly, while MnRu NPs in Mn_xRu_{100-x}@SILP catalysts are poorly alloyed, the catalytic trends observed here (i.e., suppression of aromatic hydrogenation activity, C═O hydrogenation favored) are very similar to those reported

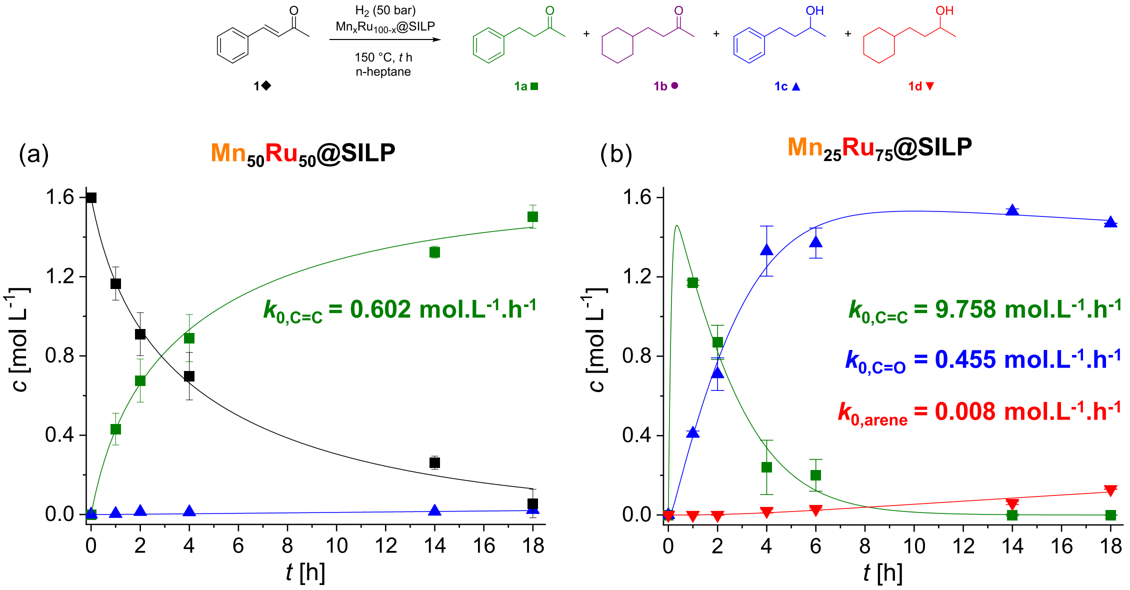

Figure 5. Time profiles recorded using (a) $Mn_{50}Ru_{50}$@SILP and (b) $Mn_{25}Ru_{75}$@SILP. Reaction conditions: Mn_xRu_{100-x}@SILP (20 mg, 0.008 mmol metals), benzylideneacetone (117 mg, 0.8 mmol, 100 equiv), 150 °C, *t* h, *n*-heptane (0.5 mL). Yields are determined via GC-FID using tetradecane as an internal standard. Experimental data was fitted using Berkeley Madonna. Solid lines are values predicted by the kinetic model. Solid points are experimental data. See SI for further details and Tables S7−S8 for the complete data sets. Data points are average values of 2−3 experiments, and error bars represent standard deviations.

for Fe_xRu_{100-x}@SILP and Co_xRu_{100-x}@SILP systems possessing alloyed bimetallic NPs (Figure S22). These results suggest that alloying is not a requirement for reactivity modulation in bimetallic structures, provided that both metals are present in the NPs. The nature of the 3d metal seems to only influence the metal ratios at which these selectivity switches occur. It is worth noting that the differences in activity and selectivity with varying Mn:Ru ratios are not correlated with a change in the oxidation state of the metals, as seen in the XAS section.

The hydrogenation performances of $Mn_{50}Ru_{50}$@SILP (selective toward **1a**), $Mn_{25}Ru_{75}$@SILP (selective toward **1c**), and $Mn_{10}Ru_{90}$@SILP (selective toward **1d**) catalysts were further investigated through the recording of time profiles (Figures 5 and S23a). Experimental results were fitted according to the kinetic equations described by Langmuir and Hinshelwood using the software Berkeley Madonna (see SI for details).[57]

Initial reaction rates for C═C, C═O and arene hydrogenation were determined, and compared to those determined by Sisodiya-Amrute et al.[34] using Fe_xRu_{100-x}@SILP and Co_xRu_{100-x}@SILP with similar selectivities under the same conditions (Table S9). At identical Ru content, the initial C═C hydrogenation rate of $Mn_{50}Ru_{50}$@SILP (0.602 mol L^{-1} h^{-1}) was found more than 2 times larger than that of $Fe_{50}Ru_{50}$@SILP (0.283 mol L^{-1} h^{-1}), although monometallic Mn and Fe NPs are both inactive for this transformation under these conditions. The activity of $Co_{90}Ru_{10}$@SILP is higher at much lower Ru content, most likely due to the intrinsic activity of Co.[34] The trend is similar for C═O hydrogenation activity, with an initial C═O hydrogenation rate 3 times higher for $Mn_{25}Ru_{75}$@SILP (0.455 mol L^{-1} h^{-1}) than for $Fe_{25}Ru_{75}$@SILP (0.154 mol L^{-1} h^{-1}). The arene hydrogenation rate of $Mn_{25}Ru_{75}$@SILP (0.008 mol L^{-1} h^{-1}) is very low, confirming again this catalyst's high selectivity toward **1c**. While contributions from NPs size and structural effects cannot be ruled out, these results suggest that the combination of Mn and Ru is particularly beneficial to modulate hydrogenation activity, especially as compared to FeRu systems. In this case, Ru is the hydrogenation-active metal, and Mn presumably facilitates the adsorption and activation of carbonyl functionalities at the NPs surface while disrupting assemblies of Ru atoms typically responsible for aromatic ring hydrogenation. $Mn_{10}Ru_{90}$@SILP (Figure S23a and Table S10) gave the fully hydrogenated product **1d** as major product (91%) after 2 h, which is similar to the activity of monometallic Ru@SILP (Figure S23b) with similar NP size (3.6 nm for both).[34] However, differences in the reaction pathway can already be observed at these low Mn concentrations: While Ru@SILP produces **1d** with **1b** as the only intermediate, the pathway for $Mn_{10}Ru_{90}$@SILP proceeds preferably over **1c**, with small amounts of **1b** also present.

Recycling experiments were carried out using $Mn_{25}Ru_{75}$@SILP (Figure S24 and Table S11) and a reaction time of 2 h. In the first reaction cycle, a mixture of **1a** (46%) and **1c** (52%) was obtained. A substantial decrease in arene hydrogenation was observed in the second cycle (20% yield of **1c**, 80% **1a**), and the reactivity was then constant up to cycle five. Elemental analysis by SEM-EDX after the first cycle revealed a decrease in total metal loading from 1.2 mol % to 1.0 mol %, mainly originating from the leaching of Ru. As a result, the Mn:Ru ratio changed from 27:73 to 37:63 (consistent with XPS data) which accounts for the change in activity of the catalyst (Table S12). The catalyst composition and performance remained stable after cycle 2. TEM and XPS analyses after cycle 5 showed no change in nanoparticle size (1.9 ± 0.4 nm, Figure S25) nor in the oxidation states of Ru and Mn (Figure S26a–b). The F 1s and N 1s XPS spectra remained consistent with those of the fresh catalyst, confirming the structural integrity and recyclability of the SILP material (Figure S26c–d).

XAS measurements of $Mn_{10}Ru_{90}$@SILP, $Mn_{25}Ru_{75}$@SILP and $Mn_{50}Ru_{50}$@SILP after catalysis (see further discussion in the SI, as well as Figures S27–34 and Tables S3–S4), indicate that Mn species retained an almost identical structure, while Ru species underwent substantial structural modifications during catalysis, resulting in a less crystallized phase and a more disordered coordination structure around the Ru species. While these data do not indicate an enrichment of the NP surface with any of the metals, they are in line with previous reports on structural changes of bimetallic materials in the presence of substrate molecules and/or H_2 at elevated temperature.[36,58,59]

3. CONCLUSIONS

A series of bimetallic MnRu NPs was synthesized on an imidazolium-based supported ionic liquid phase (Mn_xRu_{100-x}@SILP). Small (1.3–3.6 nm), well-dispersed and bimetallic NPs were observed for all Mn:Ru ratios. X-ray absorption spectroscopy revealed oxidized Mn and metallic Ru species in a negligible alloying state. The catalytic properties of Mn_xRu_{100-x}@SILP were explored in the hydrogenation of benzylideneacetone (**1**) as a model reaction. The incorporation of even small amounts of Mn in Ru NPs (e.g., 10%) was sufficient to favor C═O hydrogenation over arene hydrogenation, as evidenced by the switch in the reaction pathway. Catalysts with Mn contents up to 15% lead to full hydrogenation of **1**, while increasing the Mn content above 25% resulted in a suppression of the arene hydrogenation, but maintained C═O hydrogenation activity. Interestingly, this trend is also typical of Fe_xRu_{100-x}@SILP and Co_xRu_{100-x}@SILP catalysts containing alloyed NPs. This indicates that the selectivity switches and synergistic effects generally observed for 3d metal-Ru bimetallic NPs do not rely on the miscibility of the two metals and do not necessitate formation of alloy-type phases. The present study shows that the tunability of the properties are not significantly impacted by the structure of as-synthesized NPs, nor by the crystallographic compatibility of the metals. While other effects cannot be excluded at this stage, we hypothesize that the effects arise from their surface composition under turnover conditions. Depending on the oxophilicity, the 3d metal is dragged toward the surface by interaction with the C═O function of the substrate, thus interrupting the facial arrangement necessary for arene hydrogenation. While further work is required to probe this assumption, the experimental observations in this work provide valuable insight into the reactivity of bimetallic 3d metal-noble metal NPs, and may help guide the design of new supported bimetallic NPs for selective hydrogenation.

■ ASSOCIATED CONTENT

Supporting Information

The Supporting Information is available free of charge at https://pubs.acs.org/doi/10.1021/acscatal.4c05494.

Synthetic procedures, characterization, and catalysis data for Mn_xRu_{100-x}@SILP catalysts and reference materials (PDF)

AUTHOR INFORMATION

Corresponding Authors

Walter Leitner − *Max Planck Institute for Chemical Energy Conversion, 45470 Mülheim an der Ruhr, Germany; Institute for Technical and Macromolecular Chemistry, RWTH Aachen University, 52074 Aachen, Germany;* orcid.org/0000-0001-6100-9656; Email: walter.leitner@cec.mpg.de

Alexis Bordet − *Max Planck Institute for Chemical Energy Conversion, 45470 Mülheim an der Ruhr, Germany;* orcid.org/0000-0003-0133-3416; Email: alexis.bordet@cec.mpg.de

Authors

Johannes Zenner − *Max Planck Institute for Chemical Energy Conversion, 45470 Mülheim an der Ruhr, Germany; Institute for Technical and Macromolecular Chemistry, RWTH Aachen University, 52074 Aachen, Germany*

Liqun Kang − *Max Planck Institute for Chemical Energy Conversion, 45470 Mülheim an der Ruhr, Germany;* orcid.org/0000-0003-2100-4310

Neha Antil − *Max Planck Institute for Chemical Energy Conversion, 45470 Mülheim an der Ruhr, Germany*

Jacob Johny − *Max Planck Institute for Chemical Energy Conversion, 45470 Mülheim an der Ruhr, Germany*

Serena DeBeer − *Max Planck Institute for Chemical Energy Conversion, 45470 Mülheim an der Ruhr, Germany;* orcid.org/0000-0002-5196-3400

Complete contact information is available at: https://pubs.acs.org/10.1021/acscatal.4c05494

Funding

Open access funded by Max Planck Society.

Notes

The authors declare no competing financial interest.

ACKNOWLEDGMENTS

The authors acknowledge financial support by the Max Planck Society and by the Deutsche Forschungsgemeinschaft (DFG, German Research Foundation) under Germany's Excellence Strategy−Exzellenzcluster 2186 "The Fuel Science Center" ID: 390919832. L.K. acknowledges the Alexander von Humboldt Foundation for a postdoctoral fellowship and funding support. J.Z. thanks the networking programme 'Sustainable Chemical Synthesis 2.0' for support and fruitful discussions across disciplines. The authors thank Elena Böhme and Aaron Kretschmer for help with experimental work and Dr. Niklas W. Kinzel for the synthesis of $[Mn[N(SiMe_3)_2]_2(THF)]$. We thank Natalia Jacobs and Johanna Taing (Max Planck Institute for Chemical Energy Conversion) for $N_2(g)$ adsorption measurements. The authors would like to thank Norbert Pfänder, Hooman Ghazi Zahedi (Max Planck Institute for Chemical Energy Conversion) and Adrian Schlüter (Max-Planck-Institut für Kohlenforschung) for TEM and STEM/EDX analysis. We thank Alin Benice Schöne (Max-Planck-Institut für Kohlenforschung) for SEM/EDX measurements. The authors are also thankful to Annika Gurowski, Alina Jakubowski, and Justus Werkmeister (Max Planck Institute for Chemical Energy Conversion) for GC and GC-MS measurements. We acknowledge DESY (Hamburg, Germany), a member of the Helmholtz Association HGF, for the provision of experimental facilities. For parts of this research carried out at PETRA III, we would like to thank Dr. Edmund Welter for assistance in using beamline P65 (Proposal No. I-20211319 and I-20230324). We thank Diamond Light Source for access and support in use of the electron Physical Science Imaging Centre (ePSIC) under proposal number MG32035 that contributed to the results presented here. We would like to thank Dr. Chris Allen, Dr. Mohsen Danaie and Dr. David Hopkinson for assistance in use of instrument E02 at ePISC during the experiment session.

REFERENCES

(1) Vilé, G.; Albani, D.; Almora-Barrios, N.; López, N.; Pérez-Ramírez, J. Advances in the Design of Nanostructured Catalysts for Selective Hydrogenation. *ChemCatChem* **2016**, *8* (1), 21−33.

(2) Tomishige, K.; Nakagawa, Y.; Tamura, M. Selective Hydrogenolysis and Hydrogenation using Metal Catalysts Directly Modified with Metal Oxide Species. *Green Chem.* **2017**, *19* (13), 2876−2924.

(3) Zimmerman, J. B.; Anastas, P. T.; Erythropel, H. C.; Leitner, W. Designing for a Green Chemistry Future. *Science* **2020**, *367* (6476), 397−400.

(4) Zhang, L.; Zhou, M.; Wang, A.; Zhang, T. Selective Hydrogenation over Supported Metal Catalysts: From Nanoparticles to Single Atoms. *Chem. Rev.* **2020**, *120* (2), 683−733.

(5) Sun, Z.; Wang, S.; Chen, W. Metal Single-Atom Catalysts for Selective Hydrogenation of Unsaturated Bonds. *J. Mater. Chem. A* **2021**, *9* (9), 5296−5319.

(6) Zhao, X.; Chang, Y.; Chen, W.-J.; Wu, Q.; Pan, X.; Chen, K.; Weng, B. Recent Progress in Pd-Based Nanocatalysts for Selective Hydrogenation. *ACS Omega* **2022**, *7* (1), 17−31.

(7) Kahsar, K. R.; Schwartz, D. K.; Medlin, J. W. Control of Metal Catalyst Selectivity through Specific Noncovalent Molecular Interactions. *J. Am. Chem. Soc.* **2014**, *136* (1), 520−526.

(8) Lindlar, H.; Dubuis, R. Palladium Catalyst for Partial Reduction of Acetylenes. *Org. Synth.* **2003**, 89.

(9) Snelders, D. J. M.; Yan, N.; Gan, W.; Laurenczy, G.; Dyson, P. J. Tuning the Chemoselectivity of Rh Nanoparticle Catalysts by Site-Selective Poisoning with Phosphine Ligands: The Hydrogenation of Functionalized Aromatic Compounds. *ACS Catal.* **2012**, *2* (2), 201−207.

(10) Corma, A.; Serna, P. Chemoselective Hydrogenation of Nitro Compounds with Supported Gold Catalysts. *Science* **2006**, *313* (5785), 332−334.

(11) Ruland, H.; Song, H.; Laudenschleger, D.; Stürmer, S.; Schmidt, S.; He, J.; Kähler, K.; Muhler, M.; Schlögl, R. CO_2 Hydrogenation with $Cu/ZnO/Al_2O_3$: A Benchmark Study. *ChemCatChem* **2020**, *12* (12), 3216−3222.

(12) Li, X.; Lin, J.; Li, L.; Huang, Y.; Pan, X.; Collins, S. E.; Ren, Y.; Su, Y.; Kang, L.; Liu, X.; Zhou, Y.; Wang, H.; Wang, A.; Qiao, B.; Wang, X.; Zhang, T. Controlling CO2 Hydrogenation Selectivity by Metal-Supported Electron Transfer. *Angew. Chem., Int. Ed.* **2020**, *59* (45), 19983−19989.

(13) Pacchioni, G. From CO_2 to Methanol on $Cu/ZnO/Al_2O_3$ Industrial Catalyst. What Do We Know about the Active Phase and the Reaction Mechanism? *ACS Catal.* **2024**, *14* (4), 2730−2745.

(14) Fouilloux, P. The Nature of Raney Nickel, its Adsorbed Hydrogen and its Catalytic Activity for Hydrogenation Reactions (Review). *Appl. Catal.* **1983**, *8* (1), 1−42.

(15) Studt, F.; Abild-Pedersen, F.; Bligaard, T.; Sørensen, R. Z.; Christensen, C. H.; Nørskov, J. K. Identification of Non-Precious Metal Alloy Catalysts for Selective Hydrogenation of Acetylene. *Science* **2008**, *320* (5881), 1320−1322.

(16) Luneau, M.; Lim, J. S.; Patel, D. A.; Sykes, E. C. H.; Friend, C. M.; Sautet, P. Guidelines to Achieving High Selectivity for the Hydrogenation of α, β-Unsaturated Aldehydes with Bimetallic and Dilute Alloy Catalysts: A Review. *Chem. Rev.* **2020**, *120* (23), 12834−12872.

(17) Mitsudome, T.; Mikami, Y.; Matoba, M.; Mizugaki, T.; Jitsukawa, K.; Kaneda, K. Design of a Silver−Cerium Dioxide Core−

Shell Nanocomposite Catalyst for Chemoselective Reduction Reactions. *Angew. Chem., Int. Ed.* **2012**, *51* (1), 136−139.

(18) Fan, C.; Zhu, Y.-A.; Zhou, X.-G.; Liu, Z.-P. Catalytic Hydrogenation of Benzene to Cyclohexene on Ru(0001) from Density Functional Theory Investigations. *Catal. Today* **2011**, *160* (1), 234−241.

(19) Bordet, A.; Moos, G.; Welsh, C.; Licence, P.; Luska, K. L.; Leitner, W. Molecular Control of the Catalytic Properties of Rhodium Nanoparticles in Supported Ionic Liquid Phase (SILP) Systems. *ACS Catal.* **2020**, *10* (23), 13904−13912.

(20) Liu, L.; Corma, A. Metal Catalysts for Heterogeneous Catalysis: From Single Atoms to Nanoclusters and Nanoparticles. *Chem. Rev.* **2018**, *118* (10), 4981−5079.

(21) Ferrando, R.; Jellinek, J.; Johnston, R. L. Nanoalloys: From Theory to Applications of Alloy Clusters and Nanoparticles. *Chem. Rev.* **2008**, *108* (3), 845−910.

(22) Alonso, D. M.; Wettstein, S. G.; Dumesic, J. A. Bimetallic Catalysts for Upgrading of Biomass to Fuels and Chemicals. *Chem. Soc. Rev.* **2012**, *41* (24), 8075−8098.

(23) Meffre, A.; Iablokov, V.; Xiang, Y.; Barbosa, R.; Fazzini, P. F.; Kelsen, V.; Kruse, N.; Chaudret, B. Influence of Chemical Composition on the Catalytic Activity of Small Bimetallic FeRu Nanoparticles for Fischer−Tropsch Syntheses. *Catal. Lett.* **2015**, *145* (1), 373−379.

(24) Qadir, M. I.; Weilhard, A.; Fernandes, J. A.; de Pedro, I.; Vieira, B. J. C.; Waerenborgh, J. C.; Dupont, J. Selective Carbon Dioxide Hydrogenation Driven by Ferromagnetic RuFe Nanoparticles in Ionic Liquids. *ACS Catal.* **2018**, *8* (2), 1621−1627.

(25) Qadir, M. I.; Bernardi, F.; Scholten, J. D.; Baptista, D. L.; Dupont, J. Synergistic CO_2 Hydrogenation over Bimetallic Ru/Ni Nanoparticles in Ionic Liquids. *Appl. Catal., B* **2019**, *252*, 10−17.

(26) Ding, K.; Cullen, D. A.; Zhang, L.; Cao, Z.; Roy, A. D.; Ivanov, I. N.; Cao, D. A General Synthesis Approach for Supported Bimetallic Nanoparticles via Surface Inorganometallic Chemistry. *Science* **2018**, *362* (6414), 560−564.

(27) Tang, Y.; Wang, H.; Guo, C.; Yang, Z.; Zhao, T.; Liu, J.; Jiang, Y.; Wang, W.; Zhang, Q.; Wu, D.; Zhao, Y.; Wen, X.-D.; Wang, F. Ruthenium−Cobalt Solid-Solution Alloy Nanoparticles for Enhanced Photopromoted Thermocatalytic CO_2 Hydrogenation to Methane. *ACS Nano* **2024**, *18* (17), 11449−11461.

(28) Bordet, A.; Leitner, W. Metal Nanoparticles Immobilized on Molecularly Modified Surfaces: Versatile Catalytic Systems for Controlled Hydrogenation and Hydrogenolysis. *Acc. Chem. Res.* **2021**, *54* (9), 2144−2157.

(29) Luska, K. L.; Bordet, A.; Tricard, S.; Sinev, I.; Grünert, W.; Chaudret, B.; Leitner, W. Enhancing the Catalytic Properties of Ruthenium Nanoparticle-SILP Catalysts by Dilution with Iron. *ACS Catal.* **2016**, *6* (6), 3719−3726.

(30) Offner-Marko, L.; Bordet, A.; Moos, G.; Tricard, S.; Rengshausen, S.; Chaudret, B.; Luska, K. L.; Leitner, W. Bimetallic Nanoparticles in Supported Ionic Liquid Phases as Multifunctional Catalysts for the Selective Hydrodeoxygenation of Aromatic Substrates. *Angew. Chem., Int. Ed.* **2018**, *57* (39), 12721−12726.

(31) Goclik, L.; Offner-Marko, L.; Bordet, A.; Leitner, W. Selective Hydrodeoxygenation of Hydroxyacetophenones to Ethyl-Substituted Phenol Derivatives using a FeRu@SILP Catalyst. *Chem. Commun.* **2020**, *56* (66), 9509−9512.

(32) Rengshausen, S.; Van Stappen, C.; Levin, N.; Tricard, S.; Luska, K. L.; DeBeer, S.; Chaudret, B.; Bordet, A.; Leitner, W. Organometallic Synthesis of Bimetallic Cobalt-Rhodium Nanoparticles in Supported Ionic Liquid Phases (Co_xRh_{100-x}@SILP) as Catalysts for the Selective Hydrogenation of Multifunctional Aromatic Substrates. *Small* **2021**, *17* (5), No. 2006683.

(33) Goclik, L.; Walschus, H.; Bordet, A.; Leitner, W. Selective Hydrodeoxygenation of Acetophenone Derivatives Using a $Fe_{25}Ru_{75}$@SILP Catalyst: A Practical Approach to the Synthesis of Alkyl Phenols and Anilines. *Green Chem.* **2022**, *24* (7), 2937−2945.

(34) Sisodiya-Amrute, S.; Van Stappen, C.; Rengshausen, S.; Han, C.; Sodreau, A.; Weidenthaler, C.; Tricard, S.; DeBeer, S.; Chaudret, B.; Bordet, A.; Leitner, W. Bimetallic M_xRu_{100-x} Nanoparticles (M = Fe, Co) on Supported Ionic Liquid Phases (M_xRu_{100-x}@SILP) as Hydrogenation Catalysts: Influence of M and M:Ru Ratio on Activity and Selectivity. *J. Catal.* **2022**, *407*, 141−148.

(35) Marchenko, N.; Lacroix, L.-M.; Ratel-Ramond, N.; Leitner, W.; Bordet, A.; Tricard, S. Bimetallic Fe_xPt_{100-x} Nanoparticles Immobilized on Supported Ionic Liquid Phases as Hydrogenation and Hydrodeoxygenation Catalysts: Influence of the Metal Content on Activity and Selectivity. *ACS Appl. Nano Mater.* **2023**, *6* (21), 20231−20239.

(36) Dupont, J.; Leal, B. C.; Lozano, P.; Monteiro, A. L.; Migowski, P.; Scholten, J. D. Ionic Liquids in Metal, Photo-, Electro-, and (Bio) Catalysis. *Chem. Rev.* **2024**, *124* (9), 5227−5420.

(37) Haumann, M.; Wasserscheid, P. SILP and SCILL Catalysis. In *Catalysis in Ionic Liquids: From Catalyst Synthesis to Application*; Hardacre, C.; Parvulescu, V., Eds.; The Royal Society of Chemistry: London, United Kingdom, 2014; pp 410−432.

(38) Jiang, T.; Zhou, Y.; Liang, S.; Liu, H.; Han, B. Hydrogenolysis of glycerol catalyzed by Ru-Cu bimetallic catalysts supported on clay with the aid of ionic liquids. *Green Chem.* **2009**, *11* (7), 1000−1006.

(39) Hellawell, A. The Constitution of Manganese Base Alloys with Metals of the Second Transition Series. *J. Less Common Met.* **1959**, *1* (5), 343−347.

(40) Raub, E.; Mahler, W. Alloys of Manganese with Platinum, Iridium, Rhodium, and Ruthenium. *Z. Metallkd.* **1955**, *46* (4), 282−290.

(41) Manyar, H. G.; Yang, B.; Daly, H.; Moor, H.; McMonagle, S.; Tao, Y.; Yadav, G. D.; Goguet, A.; Hu, P.; Hardacre, C. Selective Hydrogenation of *α,β*-Unsaturated Aldehydes and Ketones using Novel Manganese Oxide and Platinum Supported on Manganese Oxide Octahedral Molecular Sieves as Catalysts. *ChemCatChem* **2013**, *5* (2), 506−512.

(42) McManus, I. J.; Daly, H.; Manyar, H. G.; Taylor, S. F. R.; Thompson, J. M.; Hardacre, C. Selective Hydrogenation of Halogenated Arenes using Porous Manganese Oxide (OMS-2) and Platinum Supported OMS-2 Catalysts. *Faraday Discuss.* **2016**, *188* (0), 451−466.

(43) Chen, S.; Huang, H.; Jiang, P.; Yang, K.; Diao, J.; Gong, S.; Liu, S.; Huang, M.; Wang, H.; Chen, Q. Mn-Doped RuO_2 Nanocrystals as Highly Active Electrocatalysts for Enhanced Oxygen Evolution in Acidic Media. *ACS Catal.* **2020**, *10* (2), 1152−1160.

(44) Annamalai, K. P.; Zheng, X.; Gao, J.; Chen, T.; Tao, Y. Nanoporous Ruthenium and Manganese Oxide Nanoparticles/Reduced Graphene Oxide for High-Energy Symmetric Supercapacitors. *Carbon* **2019**, *144*, 185−192.

(45) Ma, Z.; Xin, Z.; Qin, S.; Huang, Y. Mn-Doped Highly Dispersed RuO2 Catalyst with Abundant Oxygen Vacancies for Efficient Decarboxylation of l-Lysine to Cadaverine. *ACS Sustainable Chem. Eng.* **2021**, *9* (40), 13480−13490.

(46) Rumble, J. R. *CRC Handbook of Chemistry and Physics*, 103rd ed.; CRC Press: Boca Raton, FL, 2022.

(47) Nuss, P.; Eckelman, M. J. Life Cycle Assessment of Metals: A Scientific Synthesis. *PLOS One* **2014**, *9* (7), No. e101298.

(48) Elangovan, S.; Topf, C.; Fischer, S.; Jiao, H.; Spannenberg, A.; Baumann, W.; Ludwig, R.; Junge, K.; Beller, M. Selective Catalytic Hydrogenations of Nitriles, Ketones, and Aldehydes by Well-Defined Manganese Pincer Complexes. *J. Am. Chem. Soc.* **2016**, *138* (28), 8809−8814.

(49) Espinosa-Jalapa, N. A.; Nerush, A.; Shimon, L. J. W.; Leitus, G.; Avram, L.; Ben-David, Y.; Milstein, D. Manganese-Catalyzed Hydrogenation of Esters to Alcohols. *Chem. - Eur. J.* **2017**, *23* (25), 5934−5938.

(50) Mukherjee, A.; Milstein, D. Homogeneous Catalysis by Cobalt and Manganese Pincer Complexes. *ACS Catal.* **2018**, *8* (12), 11435−11469.

(51) Schlichter, P.; Werlé, C. The Rise of Manganese-Catalyzed Reduction Reactions. *Synthesis* **2022**, *54* (03), 517−534.

(52) Zenner, J.; Tran, K.; Kang, L.; Kinzel, N. W.; Werlé, C.; DeBeer, S.; Bordet, A.; Leitner, W. Synthesis, Characterization, and

Catalytic Application of Colloidal and Supported Manganese Nanoparticles. *Chem. - Eur. J.* **2024**, *30*, No. e202304228.

(53) Gražulis, S.; Chateigner, D.; Downs, R. T.; Yokochi, A. F.; Quirós, M.; Lutterotti, L.; Manakova, E.; Butkus, J.; Moeck, P.; Le Bail, A. Crystallography Open Database - An Open-Access Collection of Crystal Structures. *J. Appl. Crystallogr.* **2009**, *42* (Pt 4), 726−729.

(54) Chastain, J.; King, R. C., Jr *Handbook of X-ray Photoelectron Spectroscopy*; Perkin-Elmer Corporation, 1992; Vol. *40*, p 221.

(55) Seo, S.; Park, J.; Kang, Y.-C. Chemical Analysis of Ionic Liquids Using Photoelectron Spectroscopy. *Bull. Korean Chem. Soc.* **2016**, *37* (3), 355−360.

(56) Fonseca, G. S.; Scholten, J. D.; Dupont, J. Iridium Nanoparticles Prepared in Ionic Liquids: An Efficient Catalytic System for the Hydrogenation of Ketones. *Synlett* **2004**, *2004* (09), 1525−1528.

(57) Kiperman, S. L. Some Problems of Chemical Kinetics in Heterogeneous Hydrogenation Catalysis. In *Studies in Surface Science and Catalysis*; Cerveny, L., Ed.; Elsevier: Amsterdam, Netherlands, 1986, Chapter 1; Vol. *27*, pp 1−52.

(58) Silva, D. O.; Luza, L.; Gual, A.; Baptista, D. L.; Bernardi, F.; Zapata, M. J. M.; Morais, J.; Dupont, J. Straightforward synthesis of bimetallic Co/Pt nanoparticles in ionic liquid: atomic rearrangement driven by reduction−sulfidation processes and Fischer−Tropsch catalysis. *Nanoscale* **2014**, *6* (15), 9085−9092.

(59) Tao, F.; Grass, M. E.; Zhang, Y.; Butcher, D. R.; Aksoy, F.; Aloni, S.; Altoe, V.; Alayoglu, S.; Renzas, J. R.; Tsung, C.-K.; Zhu, Z.; Liu, Z.; Salmeron, M.; Somorjai, G. A. Evolution of Structure and Chemistry of Bimetallic Nanoparticle Catalysts under Reaction Conditions. *J. Am. Chem. Soc.* **2010**, *132* (25), 8697−8703.